Climate Dynamics (2002) 18: 661–673
DOI 10.1007/s00382-001-0203-y

A.F. Carril · C.G. Menéndez · M.N. Nuñez · H. Le Treut

Mean flow-transient perturbation interaction in the Southern Hemisphere: a simulation using a variable-resolution GCM

Received: 27 November 2000 / Accepted: 13 September 2001 / Published online: 12 January 2002

Abstract The ability of an atmospheric general circulation model to reproduce fundamental features of the wintertime extratropical Southern Hemisphere (SH) circulation is evaluated with emphasis on the daily variability of the SH mean flow and the mean flow-transient perturbations interaction. Two 10-year simulations using a new version of the LMDZ GCM with a stretched grid scheme centered at 45 °S and forced by climatological SST are performed: a high (144 × 73) and low (64 × 33) horizontal resolution runs. The performance of both simulations was determined by comparing several simulated fields (zonal wind, temperature, kinetic energy, transient eddy momentum and heat fluxes, Eliassen-Palm fluxes, Eady growth rate and baroclinic conversion term) against the European Centre for Medium Range Weather Forecast reanalyses (ERA). High and low-resolution simulations are similar in many respects; in particular, both experiments reproduce the main patterns of the southern extratropical large-scale circulation satisfactorily. Increasing resolution does not improve universally some spurious aspects of the low resolution simulation (e.g. the cold bias in the high polar troposphere, the debilitated subtropical jet, the low baroclinic conversion rate). Those aspects present little sensitivity to the model resolution. The interaction between transient eddies and zonal mean flow are examined. The low-resolution experiment is able to qualitatively represent the acceleration/deceleration of the mean flow by transient perturbations, south/north of 30 °S with an accuracy similar to that of the high-resolution experiment. Although both experiments represent the baroclinic structure of the mean flow satisfactorily, the model underestimates some transient properties due to the underestimation of the baroclinic conversion term in middle latitudes. Such misrepresentation does not improve with increasing resolution and is related to the relatively weak meridional temperature gradient and the inadequate geographical distribution of the eddy heat fluxes. In particular, the eddy kinetic energy is always underestimated. Eddy kinetic energy does not improve convincingly with increasing resolution, suggesting that the adequate representation of the storm tracks is highly influenced by the physical parametrizations.

A.F. Carril (✉) · C.G. Menéndez · M.N. Nuñez
Centro de Investigaciones del Mar y la Atmósfera (CIMA, CONICET-UBA), Buenos Aires, Argentina
E-mail: a.carril@isao.bo.cnr.it

H. Le Treut
Laboratoire de Météorologie Dynamique (LMD, CNRS), Paris, France

Present address: A.F. Carril
Istituto di Scienze dell'Atmosfera e dell'Oceano, ISAO-CNR, Bologna, Italy

1 Introduction

As the available computer power has steadily increased over the last two decades, the issue of atmospheric general circulation models (GCM) resolution has been constantly revised, from the pioneering studies of Manabe et al. (1970) or Wellck et al. (1971), to the development of the present generation of climate and forecast models (e.g., Gates et al. 1995; Senior 1995; Williamson et al. 1995; Stratton 1996; Jones et al. 1997; Boer and Denis 1997). However, low-resolution models are still being used to perform very long-term climate simulations at the scale of centuries or millennia, and to conduct paleoclimatic and climate change studies. Low-resolution models can also be integrated using workstations. As a consequence, a broader scientific community, particularly from developing countries and small laboratories, can be more directly involved in the study of climate variability and sensitivity. In order to interpret adequately the output of these experiments it is necessary to assess how the models are currently performing. While increasing resolution would improve

the simulation of the transient high-frequency eddies, low-resolution GCM may provide guidance in the study of the synoptic circulation in the southern extratropics.

Although the simulation of the Southern Hemisphere (SH) extratropics has been steadily improving since the 1980s, with a better representation of the circumpolar trough and the wave 3 structure (Simmonds 1990), the contribution of increased resolution to this better behavior is not clear. According to Chen and Bromwich (1995) horizontal resolution of at least 4° by 4° seems to be indispensable for accurate simulation of the circumpolar trough. In particular, a higher resolution involves a better representation of the Antarctic and Andean topography. However, other studies suggest that even the coarse-resolution models can represent the dynamics of the mid- to high southern latitudes, including many aspects of synoptic weather systems, with useful accuracy (e.g., Tzeng et al. 1993). Although high-resolution models generally present much improved simulations in the tropics and subtropics and a strengthening and poleward shift of the circumpolar trough, very high-resolution models tend to generate too strong westerlies (Whetton et al. 1996; Jones et al. 1997). The resolution at which model performance begins to deteriorate is not completely obvious. In principle, a better resolution reduces the numerical errors and increases the number of modes that are explicitly resolved, inducing a better representation of the interaction between different scales.

The aim of the present experiments is to test the ability of the Laboratoire de Météorologie Dynamique (LMD) GCM over the Southern Ocean, making use of the flexibility of configuration allowed by the LMDZ version (Z stands for "zoom"). This model version allows one to downscale the simulations by defining a variable grid spacing in order to increase the resolution over a specific region of interest. The SH circulation is characterized by weak thermal asymmetries in the zonal direction, strongly zonal storm tracks and the dominance of the transient eddy fluxes (the role of the quasi-stationary waves in transporting heat and momentum is reduced). Kushnir and Wallace (1989) suggest that the weaker asymmetry in the boundary forcing renders the low-frequency SH winter circulation particularly sensitive to scale interactions. Then, the appropriate simulation of the transient quantities, which modulate the variance and covariance between u, v and T, plays a key role in the behavior of a GCM in the southern extratropics. Enhancing meridional resolution appears to be a natural choice for studies in the Southern Ocean, where the meridional resolution is determinant for the simulation of the eddy momentum fluxes, while high zonal resolution may not be essential (Held and Phillips 1993). Experiments presented here were built along these ideas. We define a stretched grid scheme by increasing resolution in latitude while keeping it constant in longitude at low and moderately high resolution.

A positive impact of using stretchable-grid models has been reported in previous studies. French and Canadian operational models are integrated with variable resolution stretched grids (Staniforth and Mitchell 1978; Courtier and Geleyn 1988; Staniforth et al. 1991; Cotê et al. 1993; Yessad and Benard 1996). Fox-Rabinovitz et al. (1997) show that downscaling using a variable resolution core improves the representation of the regional scales for short-term integrations and also for medium-range and long-term experiments. Déqué and Piedelièvre (1995) have used a spectral stretchable GCM for a 10-year climate simulation over Europe. Krinner et al. (1997) using a stretched grid version of the LMDZ GCM have studied the Antarctic climate.

The present work is organized as follows. A description of the model is presented in Sect. 2. The experiment's design and methodology are described in Sect. 3. Results, outlining the maintenance of the zonal-mean circulation and the relationship between the simulated zonal-mean flow and the mean transports by transient baroclinic eddies (as described by Trenberth 1991) are discussed in Sect. 4. Final remarks are in Sect. 5.

2 Model description

The atmospheric model used for the present work is the first release of the LMDZ model (called LMDZ-1). The model is based on the same formulation of the original LMD GCM (Sadourny and Laval 1984), but the horizontal discretization is defined in a flexible way through the choice of two functions which define the grid in latitude and longitude respectively. Thus, a stretched grid or zoom can be applied to any region of the globe. The atmospheric primitive equations are solved on an Arakawa C grid. Model vertical discretization is on sigma levels.

The physical parametrizations of LMDZ-1 are comprehensive but simple. The convective parametrization is a combination of the moisture adjustment scheme (Manabe et al. 1965) and the Kuo (1965) scheme. Cloud liquid water is a prognostic variable of the model. At present, the clouds created by convection are not considered. Only those associated with stratiform precipitation are taken into account. Partial condensation is allowed through a statistical approach (Le Treut and Li 1991). The radiative transfer code is derived from the approach of Fouquart and Bonnel (1980) for solar radiation and by Morcrette (1991) for longwave radiation. In the current experiments, the diurnal cycle of insolation is not taken into account. The radiation code is used at every physical time step to calculate the influence of clouds. However, the clear-sky transmission coefficients are evaluated only every four hours. Gravity wave drag is not parametrized. For the surface moisture, a bucket model with holding capacity fixed at 150 mm is considered. All the water above this value is lost as runoff. The calculation of surface temperature is incorporated in the boundary layer and is based on a surface energy balance equation.

3 Experiment design and methodology

A novel aspect of the model is the stretched grid. The stretching scheme was introduced only in the meridional direction in order to improve the resolution over a latitudinal belt of the SH charac-

terized by large gradients of circulation. To briefly illustrate the impact of defining a grid deformed in the meridional direction, we present a series of preliminary experiments. Four-year experiments were integrated with a regular grid but also with a stretched scheme as shown in Fig. 1: zoom centered at 30 °S (Z30, Fig. 1a) (i.e., the mean position of the subtropical jet) and zoom centered at 45 °S (Z45, Fig. 1b) (i.e., just between the subtropical jet and the polar jet over the Pacific Ocean and coincident with the largest meridional sea level pressure gradient). All the experiments were conducted in high (HR, 144×73; i.e., 144 points in the longitudinal direction and 73 points in the meridional direction) and low (LR, 64×33) horizontal resolution and 11 unevenly distributed sigma vertical levels.

Figure 2 displays the zonal wind component at 300 hPa, for ERA and the three LR experiments. A double westerly wind maximum over the western Pacific Ocean and a single jet over the Atlantic and Indian oceans are the main features of the observed field (Fig. 2a). Deficiencies in the simulation of the split jet structure are frequent in low-resolution (e.g. Xu et al. 1990; Katzfey and McInnes 1996), high-resolution (e.g. T63; Boville 1991) and very high-resolution (e.g., T106; Stendel and Roeckner 1998) GCMs. Then, zonal wind is a good field to illustrate the impact of defining a zoom. When model is integrated in a regular grid, the jet presents a strong zonally symmetric structure (Fig. 2b). Zonal wind field from Z30 (Fig. 2c) is somewhat better than those from the regular grid experiment. In particular, Z30 improves the magnitude of the simulated subtropical jet in the western South Pacific region while the maximum wind axis acquires a SW-NE horizontal tilt in the surroundings of Australia. However Z45 optimizes the representation of the wintertime jet split (Fig. 2d). Note in particular, the capability of the Z45 experiment to reproduce the midlatitude jet in the Indian Ocean, the entrance of the subtropical branch in the split region, the minimum over the New Zealand region, as well as the magnitude of the zonal winds in the western boundaries of the South Atlantic Ocean. At high resolution, zonal wind field from Z45 and Z30 also improve when compared with the regular grid experiment (figure not shown). Moreover, the model at HR is capable of adequately simulating the zonal wind field from both, Z45 and Z30 experiments. The reason why a zoom with center at 45 °S was chosen is the computational cost of the experiment (the integration with a zoom centered at 45 °S satisfies the CFL criterion, see Courant et al., 1928, using a larger dynamics time step than that required if the zoom is centered at 30 °S).

After determining that Z45 discretization optimizes our simulations, two 10-year experiments, with zoom centered at 45 °S, were performed: the control experiment (the higher-resolution one; HR), integrated using 144×73 points to define the horizontal mesh and the lower-resolution experiment (LR), with 64×33 horizontal grid points. The maximum meridional resolution is around 45 °S (about 1.2° at HR and 2.8° at LR) and the respective longitudinal resolutions are 2.5° and 5.625° in every case. The worst meridional resolution is in the northern midlatitudes, and it is about 3.5° at HR and 8.5° at LR experiments. Through our definition of the stretched grid we gain resolution over the main baroclinic region of the Southern Hemisphere. Experiments were designed under a rigorous sensitivity hypothesis. In particular, we fixed the vertical resolution at 11 layers and diffusion was not adjusted with resolution.

The orography at the bottom boundary of the model was derived from a data set provided by the US Navy with 1/6° of resolution. Sea surface temperature and sea-ice distributions are AMIP climatological values (Gates 1992), consisting of mean values (1979–1995) with 1° resolution. AMIP data are interpolated to daily values using a spline scheme and to the model grid using an area-weighted scheme. Initial conditions were set to July 1 1988 (ECMWF analyses) and the simulations were run for ten and a half years. The simulated fields are seasonally averaged from daily samples and analyses are done for winter (June–July–August, JJA). The observed climatology used for model validation is the ERA data set, globally gridded ($2.5° \times 2.5°$), for the period 1982–1993.

As in Peixoto and Oort (1992), we split the total zonal average kinetic energy [K] into components associated with the mean circulation [KM], the stationary [KSE] and the transient [KTE] perturbations respectively:

$$[K] = \tfrac{1}{2} \cdot [\overline{u^2} + \overline{v^2}] \tag{1}$$

$$[KM] = \tfrac{1}{2} \cdot ([\bar{u}]^2 + [\bar{v}]^2] \tag{2}$$

$$[KSE] = \tfrac{1}{2} \cdot [\bar{u}^{*2} + \bar{v}^{*2}] \tag{3}$$

$$[KTE] = \tfrac{1}{2} \cdot [\overline{u'^2} + \overline{v'^2}] \tag{4}$$

We follow a classical notation: the stars/primes denote departure from the zonal/time average, brackets indicate zonal average and over-bars note temporal mean of a given season over the whole 10 years. Transient contributions due to the interannual variability are included. As the stationary eddies are inefficient to transport mass or energy in the SH (e.g., van Loon and Jenne 1972; van Loon 1979; Trenberth 1980), the attention of the present study is focused on the activity of transient perturbations, which is then the main component at mid-latitudes in the SH (e.g., Trenberth 1981; James 1994), and the main feature which a model needs to reproduce. These transient fluxes are diagnosed as the difference between the mean term and the covariance term (Peixoto and Oort 1992). For zonal momentum and temperature the corresponding equations read:

$$\overline{u' \cdot v'} = \overline{u \cdot v} - \bar{u} \cdot \bar{v} \tag{5}$$

$$\overline{T' \cdot v'} = \overline{T \cdot v} - \bar{T} \cdot \bar{v} \tag{6}$$

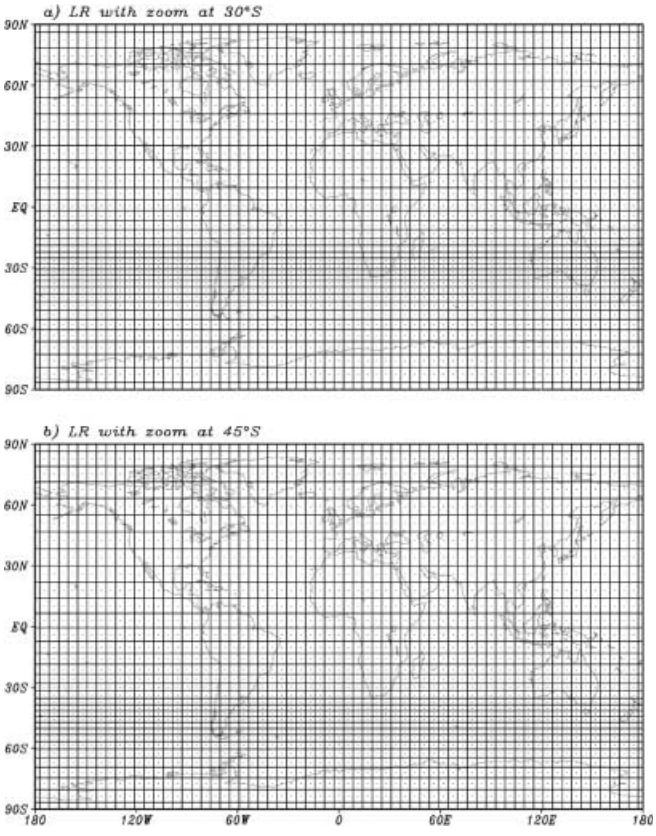

Fig. 1 Global stretched meridional grid with the area of finest resolution centered at **a** 30 °S and **b** 45 °S

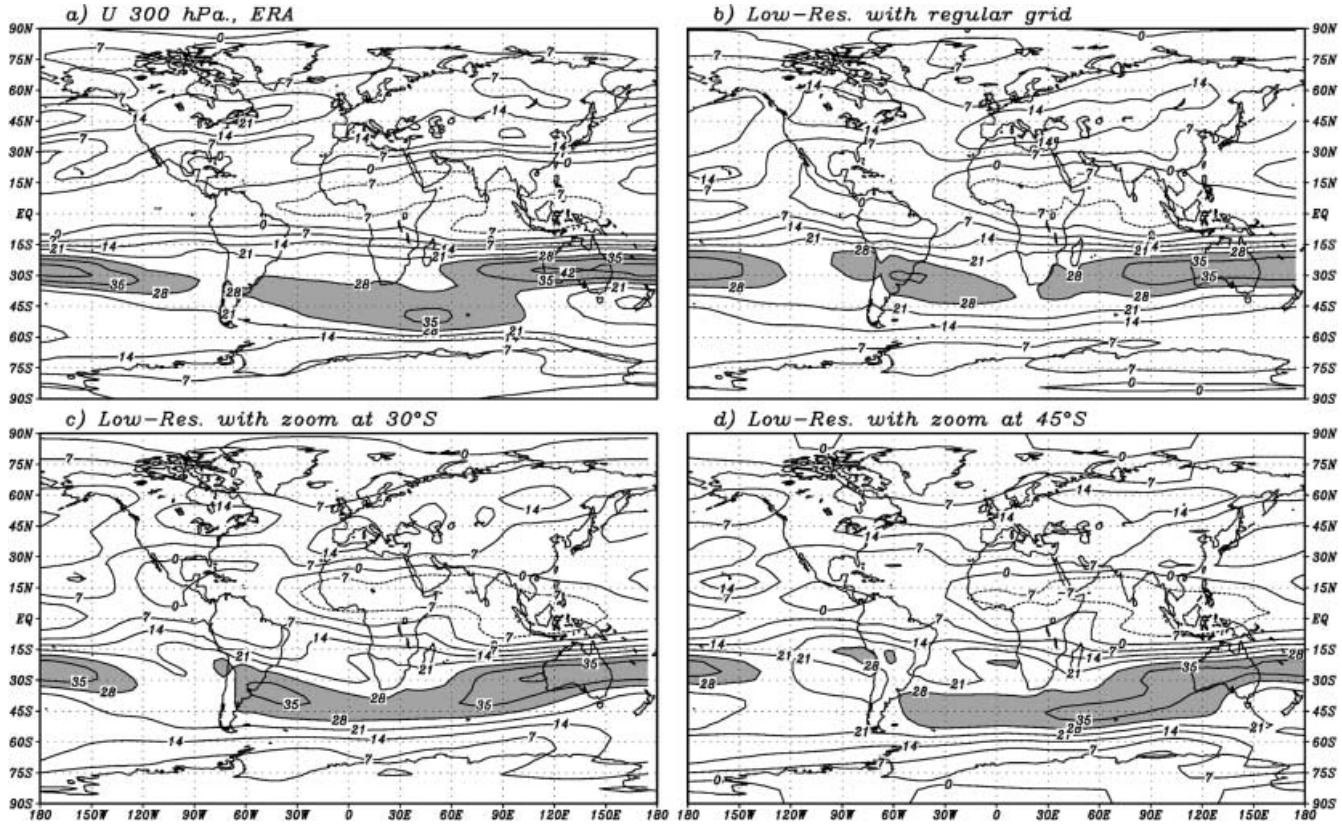

Fig. 2 Zonal wind field at 300 hPa for **a** ERA, **b** LR-regular grid, **c** LR-Z30 and **d** LR-Z45 experiments. Contours are every 7 m/s. *Gray shading* indicate the values greater than 28 m/s

4 Results

4.1 Zonal wind and temperature

Figure 3 presents the zonal-mean distribution of temperature and westerly winds obtained from the HR and LR experiments. As geostrophy is important in the SH, a main feature in simulating the extratropical climate is a correct representation of the overall tropospheric temperature structure. An inadequate tropospheric heating can produce an erroneous meridional midtropospheric temperature gradient and, consequently, a misrepresented extratropical circulation (Meehl and Albrecht 1988). In common with other atmospheric GCMs, LMDZ presents a cold bias over a major part of the troposphere. This misrepresentation is especially evident in the upper levels in the high southern latitudes, both for the HR and LR simulations, but increases with the resolution. At both resolutions, the model underestimates the intensity of the subtropical jet (centered at 30 °S and 200 hPa in the observations) and overestimates the polar jet (vertical axis of wind maximum near 50 °S in the simulation).

4.2 Kinetic energy

Zonally averaged mean-flow kinetic energy (*KM*; Fig. 4a, b) presents a maximum in the upper troposphere near 30 °S, related to the wintertime subtropical jet, and a higher latitude maximum throughout the troposphere near 50 °S, associated with the polar jet. Both, *KM* and the transient eddy kinetic energy (*KTE*; Fig. 4c, d) are the main contributors to the total kinetic energy field in the SH (field not shown).

The strong westerly jet in the upper troposphere (with the associated wind shear) and the meridional temperature gradient at middle latitudes both provide the energy source for the growth of baroclinic disturbances in the mean zonal flow. Nevertheless, because *KM* is underestimated in the simulation, there is less available energy to be transformed into *KTE*. The *KTE* from ERA presents an elongated maximum in the 30 °S–50 °S latitude belt at high levels associated with the daily to seasonal variability of the jet and the variability of the height of the tropopause (Stratton 1996). It is a measure of the storm track activity and characterizes the amount of energy associated with the transient weather systems. The model underestimates the *KTE* in the upper troposphere, especially in the subtropical region, and concentrates it farther poleward, underpredicting the strength of the subtropical jet. Traditionally, low resolution models fail to simulate the magnitude of the *KTE* which is strongly sensitive to the model resolution (e.g., Boville 1991; Boyle 1993; Williamson et al. 1995; Phillips et al. 1995; Stratton 1996). Simulated *KTE* in the upper troposphere is about 50% weaker in LR (Fig. 4g) and

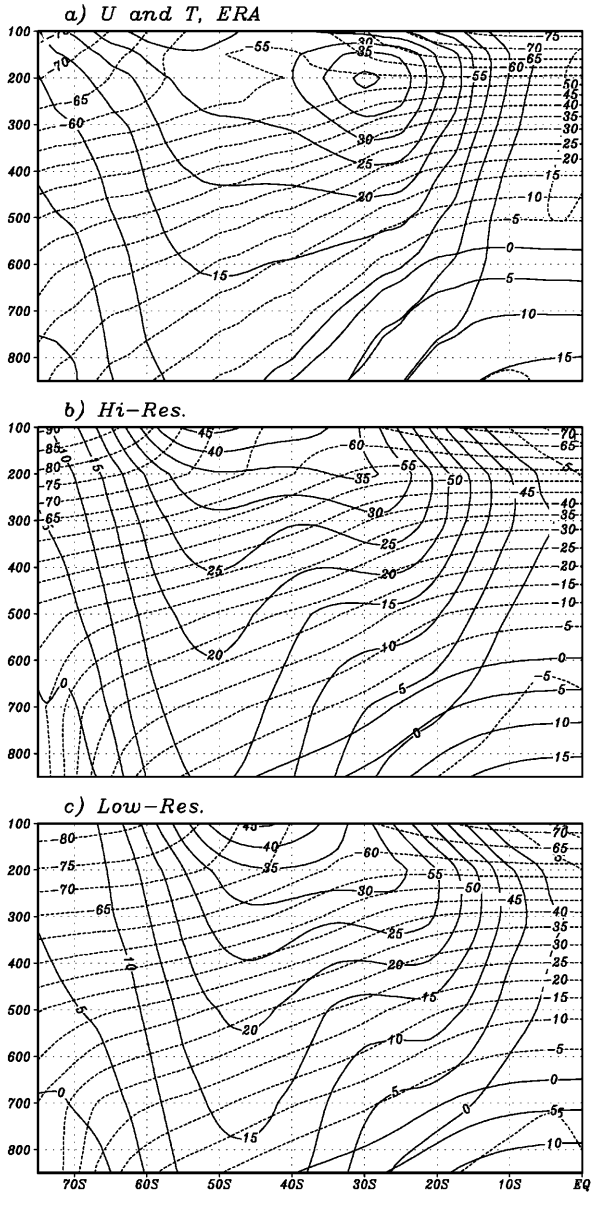

Fig. 3 Zonal mean vertical distribution of zonal wind and temperature from **a** ERA, **b** HR and **c** LR. Vertical axis is in hPa. Contour spacing is 5 m/s for the zonal wind and 5 °C for the temperature. Negative values are shown by *dashed lines*

about 35% weaker in HR (Fig. 4d) than in the ERA data (Fig. 4c). This comparison suggests that the intensity of the storm track is influenced by other factors besides the horizontal resolution (more directly associated with the model physics). In addition, the maximum in LR is located farther equatorward (near 45 °S), giving better agreement with the observational analyses. On the contrary, simulation of *KTE* in lower levels is satisfactory. Because *KTE* in the low troposphere is representative of the high-frequency transients that are more closely related to the transient weather producing systems (highs and lows), results suggest that the model is capturing the strength of these transient weather systems appropriately. The contribution of the stationary eddy kinetic energy (*KSE*; Fig. 4e, f) plays a very minor role. The overall pattern is quite well simulated although the magnitude of the upper-level waves is somewhat underestimated in the tropical region.

4.3 Momentum and heat fluxes

The meridional fluxes carried by the transient eddies of the mid-latitudes at all timescales play a key role in establishing the time mean atmospheric circulation. The mediocre skill of various GCMs in the SH extratropics has often been ascribed to the coarse horizontal resolution which alters the momentum fluxes (and, to a lesser extent, the heat fluxes) by the transients and the storm tracks (Boville 1991; Held and Phillips 1993; Stephenson and Held 1993). Zonally averaged transient eddy meridional fluxes of westerly momentum and temperature for ERA, HR and LH are displayed in Fig. 5. The eddy momentum flux (left column) is poleward in mid-latitudes and stronger near 250 hPa in the southern flank of the subtropical jet. The magnitude of the maximum transient momentum flux at HR is similar to, but slightly weaker than, the ERA climatology (at LR the maximum is still weaker). In the lower half of the troposphere, the model always tends to overestimate the strength of the eddy momentum flux. At high latitudes (south of 55 °S), the fluxes are equatorward both in the model and the analyses. Therefore westerly momentum converges near the region of the circumpolar trough and is redistributed in the vertical by the Ferrel cell. The latitude of the convergence is appropriately captured. The magnitude of the poleward transport at LR is slightly less than at HR.

The poleward transient heat flux (right column) is largest in the lower troposphere at the storm track latitudes. This maximum is caused primarily by closed cyclonic/anticyclonic disturbances and fronts. A secondary maximum, associated with open waves, is located at 200 hPa. The transient systems are responsible of the meridional exchange of different air masses. Over time, transient eddy fluxes act to reduce baroclinicity by dissipating anomalies in the temperature field. Thus, the effect of eddies is to cool the tropics and subtropics and to warm the high latitudes, thereby reducing the meridional temperature gradient. The model overestimates the magnitude of this eddy property in the lower levels (especially at HR) and the simulated maximum is located somewhat south of its observed position. Furthermore, the model does not capture the secondary maximum in high levels, perhaps due to its coarse vertical resolution, particularly in the upper troposphere and stratosphere.

4.4 Transient eddies-mean flow interaction

The Eliassen-Palm (EP) flux is used as a diagnostic of the mean forcing of the zonal-mean flow by the eddies.

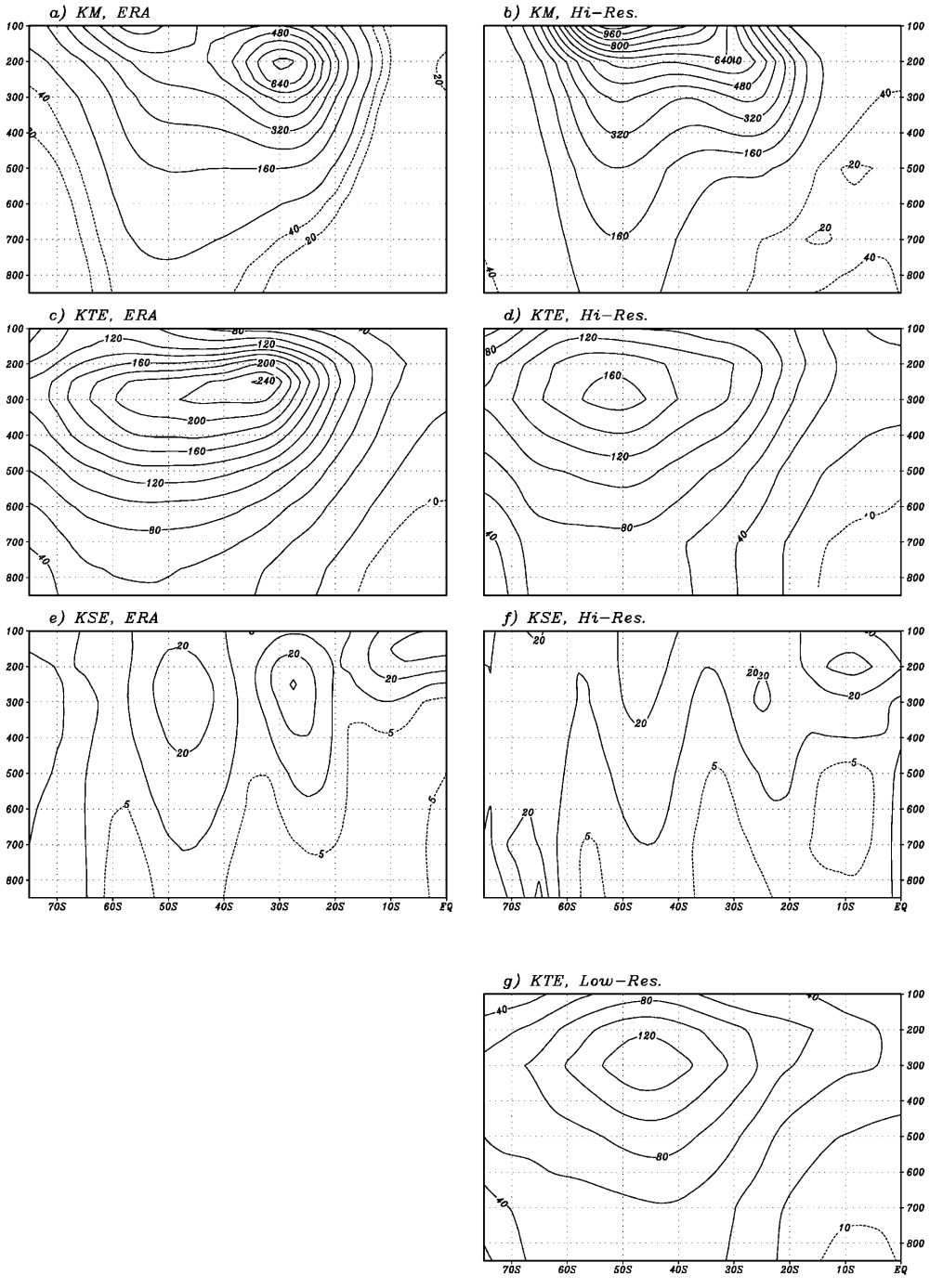

Fig. 4a–g Latitude-pressure cross sections of mean kinetic energy (*KM*), transient eddy kinetic energy (*KTE*) and stationary eddy kinetic energy (*KSE*). *Left column* is for ERA and the *right one* for HR experiment (apart from the *bottom diagram* which is for LR). *Vertical axis* is in hPa. Contours are every 80 m^2/s^2 for *KM*, every 20 m^2/s^2 for *KTE* and every 10 m^2/s^2 for *KSE*. Extra contours are shown by *dashed lines* and spacing are 20 m^2/s^2 for *KM*, 10 m^2/s^2 for *KTE* and 5 m^2/s^2 for *KSE*

The EP flux divergence is largest in the upper troposphere, indicating that the mean flow is modified in this region by the effects of the propagating transient disturbances. Following Hoskins et al. (1983) the horizontal EP flux (vector $\mathbf{E}_u$) is defined as:

$$\mathbf{E}_u = \left[\tfrac{1}{2}\cdot(\overline{v'^2} - \overline{u'^2}), -\overline{u'v'}\right] \quad (7)$$

In the regions where $\mathbf{E}_u$ diverges, the transient eddies interact with the mean flow, intensifying the westerlies (details are given in Trenberth 1986).

Figure 6 shows the zonally averaged divergence of $\mathbf{E}_u$ vector at 300 hPa for ERA, HR and LR experiments. The interaction between the transient disturbances and the zonal mean flow in the mid- to high southern latitudes is quite accurately simulated. The $\mathbf{E}_u$ vector diverges/converges south/north of about 32 °S where eddies barotropically accelerate/decelerate the zonal mean flow. Nevertheless, the simulated extremes are slightly weak and the position of the maximum divergence in the mid-latitudes lies too far south. Transient eddies-mean flow interaction is weaker in LR than in

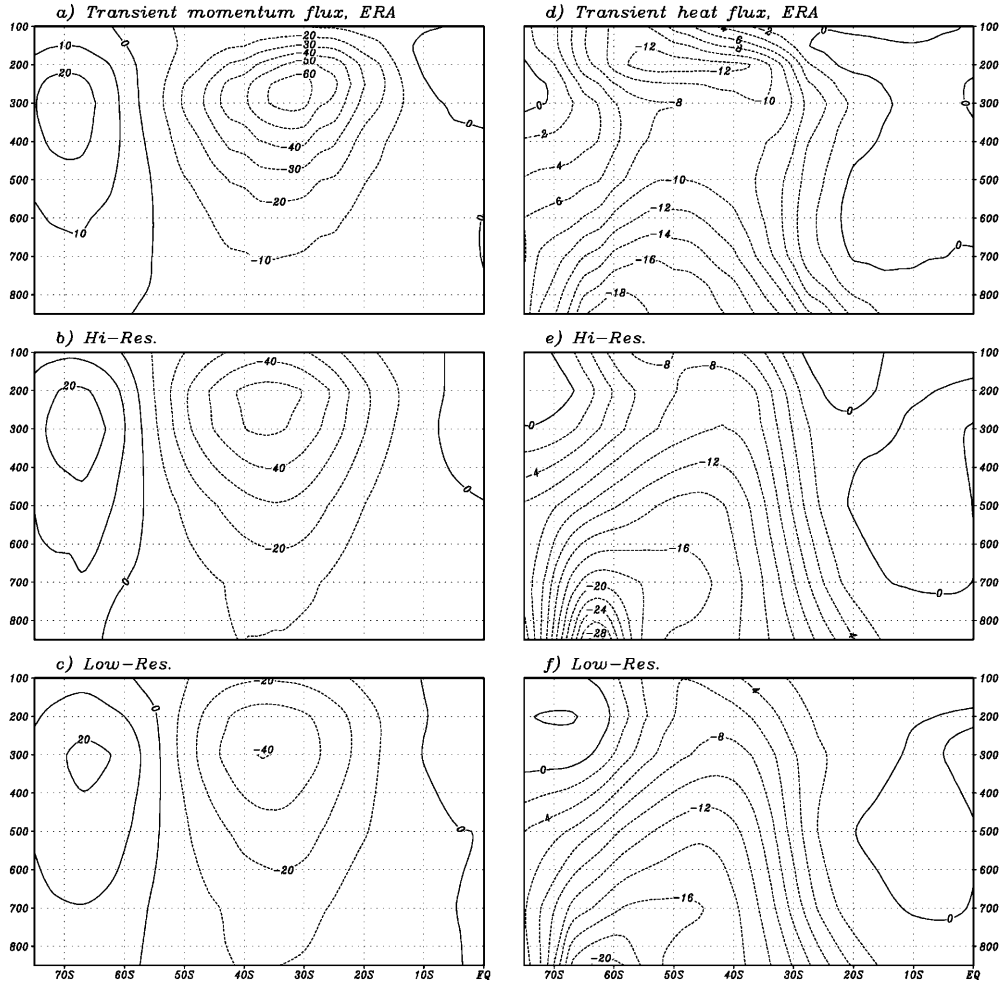

Fig. 5a–f Latitude-pressure cross sections of transient eddy momentum (*left column*) and heat (*right column*) fluxes. *Top panels* are for ERA, *middle panels* for HR and the *bottom panels* for LR experiment. *Vertical axis* is in hPa. Contour spacing is 10 m^2/s^2 for momentum and 2 °Cm/s for heat fluxes

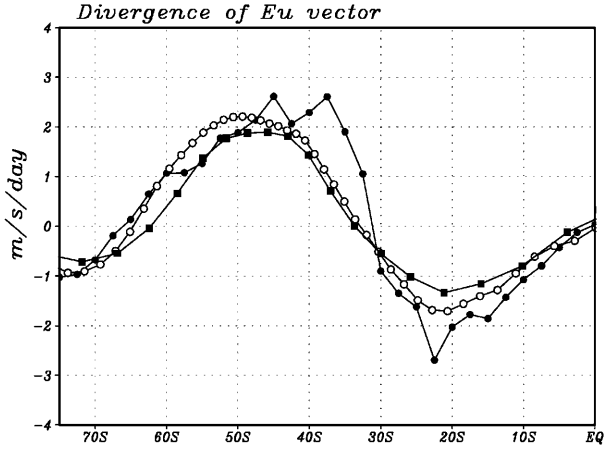

Fig. 6. Zonal mean average of the horizontal divergence of $\mathbf{E}_u$ vector at 300 hPa as a function of the latitude. *Open circles* are for HR, *solid squares* for LR and *solid circles* for ERA data sets. *Vertical axis* is in m/s/day

HR. In particular, the latitude of the maximum divergence is better approximated by the coarse resolution experiment, in agreement with a better representation of the mean zonal flow in high latitudes (the westerlies are less overestimated in the LR than in the HR experiment). At HR the transient perturbations tend to intensify the polar jet too much.

4.5 Baroclinic processes

Because variances and covariances in the SH are dominated by the contribution of the transient high-frequency eddies (Trenberth 1981) associated with baroclinic processes (Hoskins et al. 1983), it is interesting to consider the capability of the model to reproduce the baroclinicity of the mean flow. A sufficiently baroclinic mean state is a necessary, but not sufficient, condition for the growth of eddies. A parameter commonly used to quantify the baroclinic instability of the mean flow is the Eady growth rate (σ), which is an indicator of the maximum values that baroclinic instability can take. Following Hoskins and Valdés (1990), the Eady growth rate is defined as:

$$\sigma = 0.31 \cdot f \cdot \left|\frac{\partial V}{\partial z}\right| \cdot N^{-1} \tag{8}$$

where f is the Coriolis parameter and N is the Brunt-Väisälä frequency. The σ depends on the vertical wind

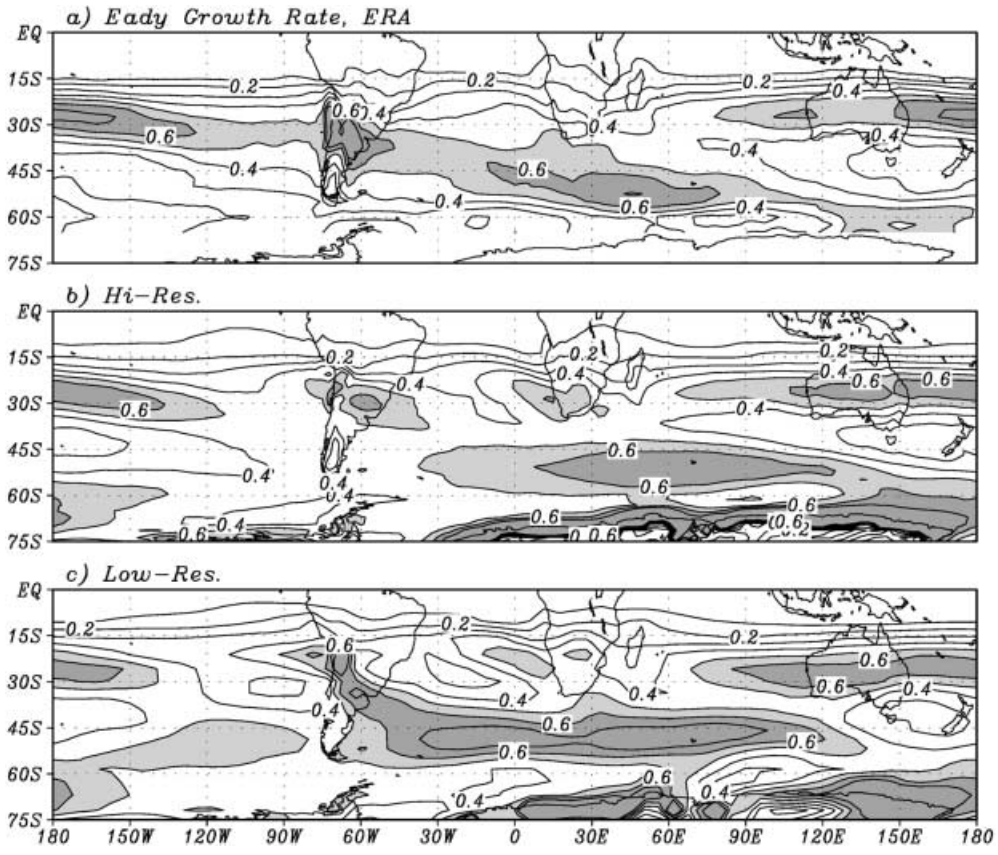

Fig. 7. **a** ERA, **b** HR and **c** LR Eady growth rate estimated for the thickness 700–500 hPa. Contours are every 0.1/day. *Light* and *dark gray shading* highlights areas with values greater than 0.5 and 0.6/day respectively

shear, the large-scale static-stability and the latitude. It is dominated by the wind shear term, which is in thermal wind balance with the meridional temperature gradient.

The characteristics of the upper level winds are reflected in regions of maximum σ (Fig. 7). In particular, the split of this field in the Eastern Hemisphere is representative of the wintertime dual jet structure. Both experiments reproduce the baroclinicity of the mean flow satisfactory, suggesting that the mean state of the model is favorable for the growing of baroclinic perturbations. In particular, LR experiment slightly overestimates baroclinicity of the mean flow in the latitude of the main storm track (~45 °S). Considerations in high latitudes are not made because it is not known whether the large values of σ over the Antarctic coasts are a real characteristic of the atmosphere or a misrepresentation related to the abrupt topography (Sinclair 1994). Although the basic state provides an adequate energy source for growing disturbances due to baroclinic instability, the simulated transient eddy kinetic energy is very weak. This fact suggests that baroclinic conversion could be misrepresented.

Let us explore the energy flow of our model. As in Orlanski and Sheldon (1995), the baroclinic conversion can be expressed as:

$$\bar{\alpha} \cdot \left(\theta \cdot \frac{\partial \theta}{\partial p} \right)^{-1} \cdot \overline{\mathbf{v}' \theta'} \cdot \nabla \theta \qquad (9)$$

where α is the specific volume and θ is the potential temperature. The baroclinic conversion term, which expresses the conversion of the mean-flow available potential energy to the eddy available potential energy, depends on the atmospheric stability and the correlation between the temperature flux and the poleward temperature gradient. It reaches maximum values at low levels, where this correlation maximizes. The model underpredicts the three peaks of baroclinic conversion along the southern mid-latitudes (downstream of the subtropical jetstream over the Pacific Ocean, downstream of South America and over the southwestern Indian Ocean) while their locations are simulated appropriately (see Fig. 8). Baroclinic conversion is slightly weaker in LR than in HR, consistent with a weaker storm track field. In the sub-Antarctic ocean, the model overestimates the baroclinic conversion, while LR gives better agreement with the observational analyses (even the geographical distribution of the baroclinic conversion around Antarctica is rather well represented in LR, with a maximum in the Australian sector and a minimum in the Weddell Sea).

To understand why this misrepresentation is occurring, two related quantities (meridional temperature gradient and eddy heat flux) are shown in Figs. 9 and 10. The large-scale distribution of the simulated meridional temperature gradient is rather well represented (Fig. 9). But the model underestimates the thermal gradient over a major part of the hemisphere between 15 °S and 60 °S.

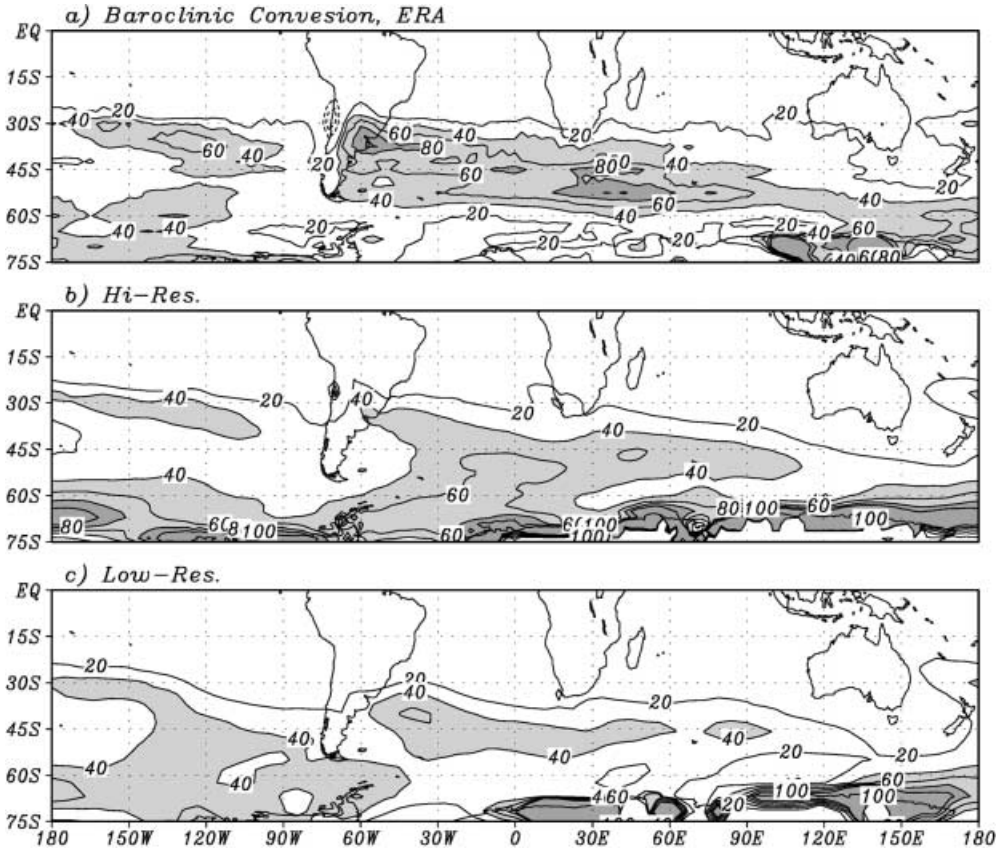

Fig. 8. **a** ERA, **b** HR and **c** LR baroclinic conversion term at 700 hPa. Contours are every 20 m^2/s^2/day. Values greater than 40 and 80 m^2/s^2/day are *light* and *dark gray shaded* respectively. Zero line is omitted

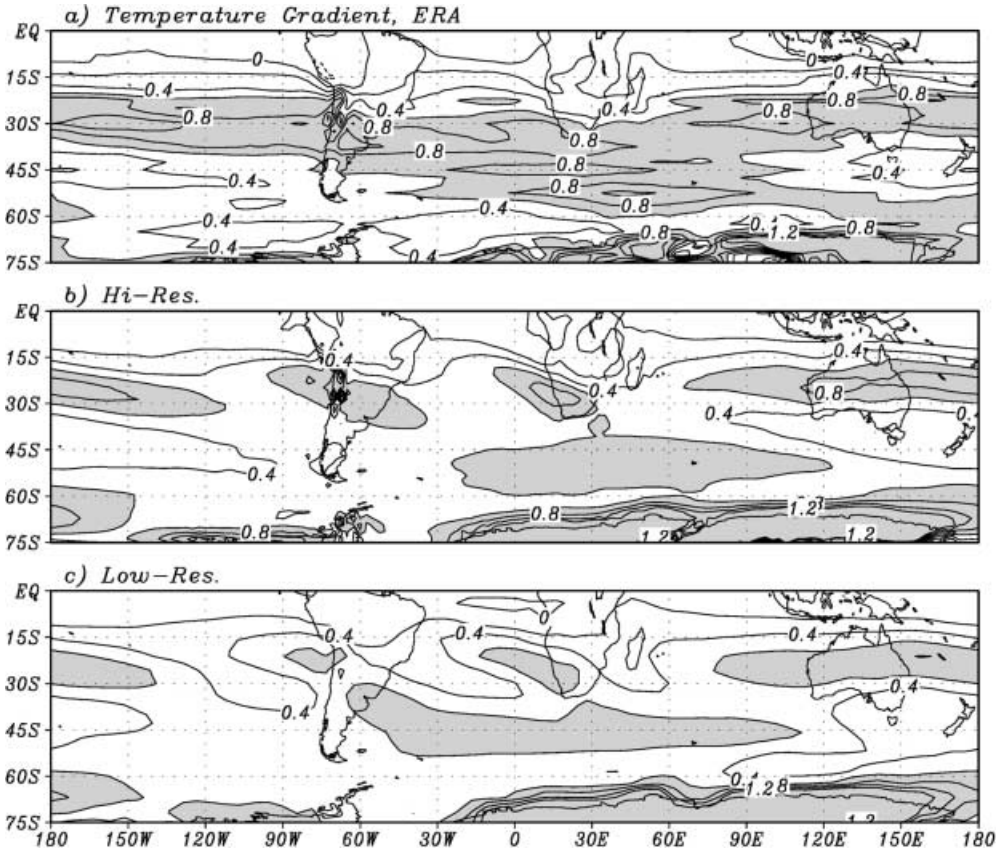

Fig. 9. **a** ERA, **b** HR and **c** LR meridional temperature gradient (every 0.2 °C/°latitude). Values greater than 0.6 °C/° latitude are *shaded*

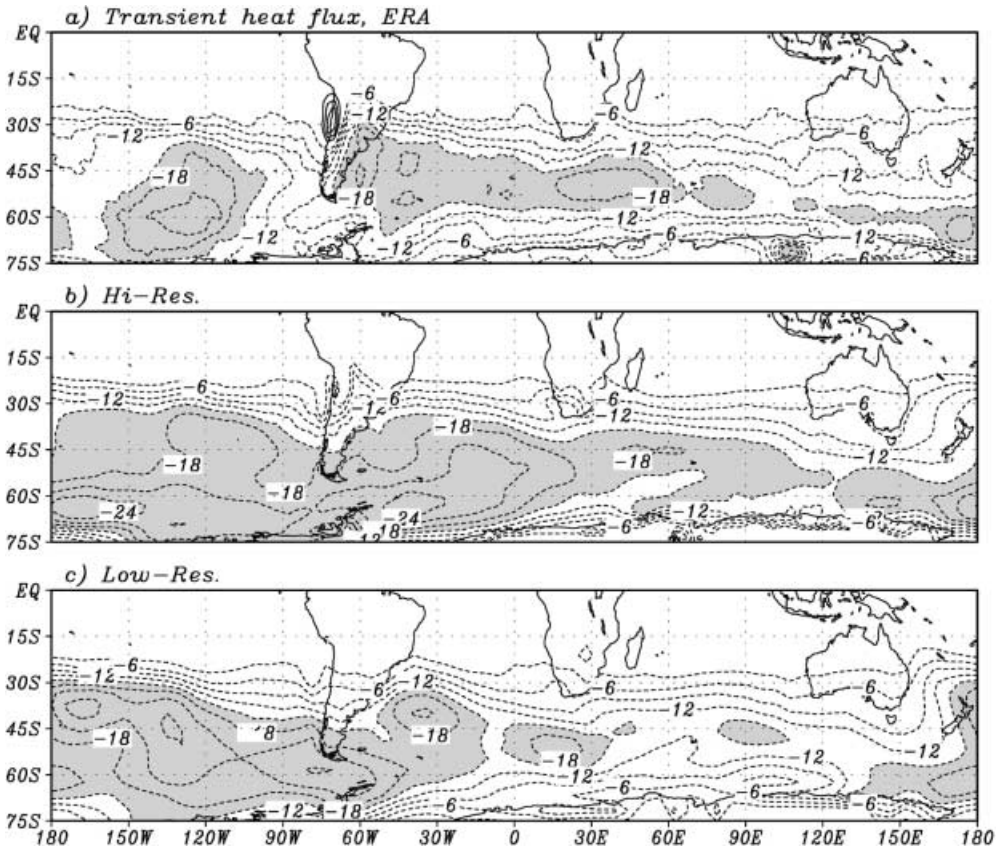

Fig. 10. **a** ERA, **b** HR and **c** LR transient eddy heat flux (every 3 °Cm/s). Values lower than –15 °Cm/s are *shaded*. Zero line is omitted

In some important regions (e.g., the main storm track region) the model significantly underpredicts this quantity. The meridional temperature gradient in LR is weaker than in HR both in the subtropics and poleward of 50 °S. In the mid-latitudes, however, the gradient is somewhat stronger in LR. Another contributor to the baroclinic conversion term is the transient eddy heat flux (Fig. 10). As mentioned before, the model tends to overestimate the meridional heat transport in the mid- to high latitudes. Thus, the simulated baroclinic eddies further reduce the meridional temperature gradient through their enhanced heat fluxes. This decreased thermal gradient implies weaker transient eddies over the southern mid-latitudes. In LR experiment, the meridional eddy heat flux is too intense over the Pacific Ocean. In contrast, around Antarctica this quantity is weaker in LR than in HR, again giving better agreement with the analyses.

There is a close relationship between the baroclinic contribution to the eddy kinetic energy generation, the meridional temperature gradient and the horizontal heat fluxes. In the simulation analyzed despite the implicit baroclinic conditions of the mean flow in the main storm track region, eddies do not develop enough due to the underestimation of the baroclinic conversion term in the middle latitudes. Such underestimation arrives from the meridional temperature gradient underestimation and also partly due to shortcomings in the simulated transient eddy heat fluxes. The baroclinic eddies reduce the meridional temperature gradient through their heat fluxes. Other processes such as surface heat fluxes and latent heating within the baroclinic eddies also affect the thermal gradient. These effects must be treated adequately in the physical parametrizations of the models.

4.6 Radiative balance

Climate simulation is attempting to balance the competing effects of the radiation budget and the instability processes. The meridional gradient of radiation constitutes the basic driving force for the atmospheric motions. Taking energy from the available potential energy of the mean flow, baroclinic perturbations act to reduce the meridional gradients that the radiative driving force tends to restore. Figure 11 presents a zonally averaged estimation of the radiative balance and the meridional gradient of transient eddy heat fluxes, at low and high-resolution. The radiative budget is estimated as the balance between the radiation at the top of the atmosphere and the surface processes (i.e., short and long wave radiation in the top of the atmosphere, radiation at surface, sensible and latent heat fluxes and the heat flux into the subsurface layers).

There is a good agreement between the divergence of transient heat fluxes and the radiative balance. Dis-

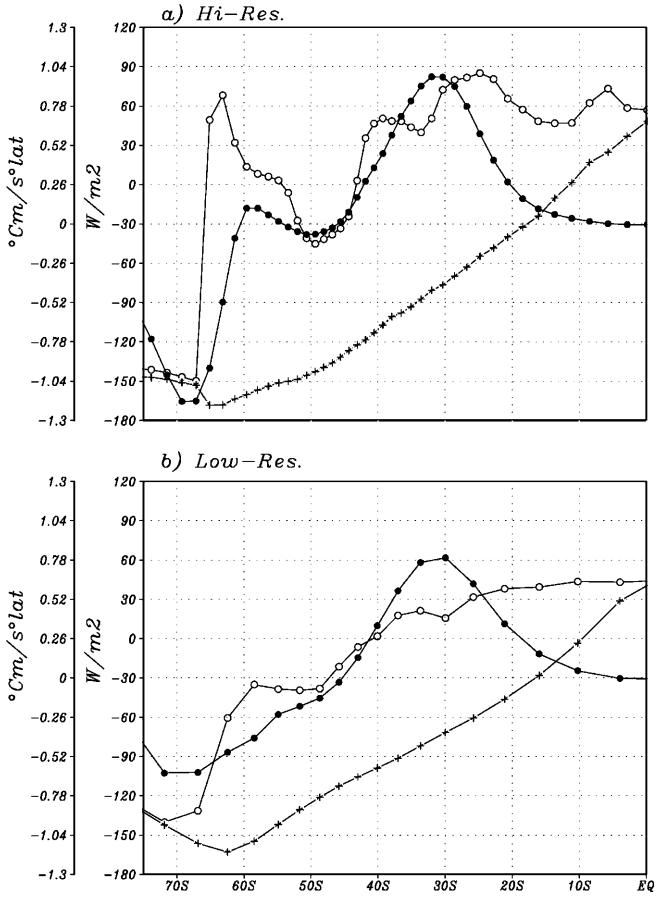

Fig. 11 Zonally averaged estimation of the radiative balance (W/m^2) at the top-of-the-atmosphere (*crosses*), radiative balance (W/m^2) including the surface processes (*open circles*) and meridional gradient of eddy heat flux (°Cm/s°latitude) vertically integrated (*solid circles*) from **a** HR and **b** LR experiments

crepancies can be caused by the inaccuracy of the diagnostics (e.g., model outputs are every 48 time steps, we are not considering the contribution of moisture fluxes, we neglect the contribution of the asymmetric eddies). Radiation balance presents moderate sensitivity to the horizontal resolution, which mainly arise from changes in the surface balance term. Note, in particular, the behavior near 60 °S and how the divergence of heat fluxes at HR peaks close to it. Heat exchange an the top of the atmosphere is not strongly modified by the model resolution, while the surface balance heat dominates the energetic constraints.

5 Final remarks

The weather and climate of the mid- to high southern latitudes are influenced by the collective tracks of individual cyclones. As the stationary waves transport little energy in the SH, much of the meridional transport in the atmosphere occurs through transient eddies, which owe their existence to baroclinic instability processes. The general circulation is characterized by strong interactions between these eddies and the mean zonal current (Pfeffer 1981). The transients are responsible for accelerating the zonal mean flow south of 35 °S, transporting momentum out of the jet stream and into the higher latitudes. On the other hand, large vertical heat fluxes into the atmosphere occur at the air-sea interface over the Southern Ocean to the north of the ice edge. The dramatic change of the turbulent surface heat fluxes over the open ocean affect the behavior of weather systems (Orlanski et al. 1991), their baroclinic structure and the overall energy budget of the atmosphere. The simulations must capture different feedback effects between the mean flow, the baroclinic transients and the energy budget. Therefore there is a need for better understanding and ability to model these processes in the SH extratropics.

The results of the HR simulation have been compared with ERA climatology and with the LR experiment. The basic features of the mean fields (including the split jet) simulated by HR, are broadly consistent with the observed, but yet present some biases (not detailed here, see Carril 1998). In common with other atmospheric GCMs (Boer et al. 1992) there is a significant cold bias over the major part of the hemisphere. A problem in the HR run is the unrealistically strong wind in the mid- to high latitudes (shortcoming also present in other very high-resolution GCMs; e.g., Whetton et al. 1996; Jones et al. 1997). The great strength of the westerlies over the Southern Ocean can affect the eddy development negatively because any growing perturbation is transported too quickly, thereby probably limiting their growth through local baroclinic instability. The upper-troposphere eddy kinetic energy remains too weak, especially between the subtropical jet and the midlatitudes, despite the high horizontal resolution of the model. This shortcoming, related to the insufficient baroclinic conversion, is mainly due to a weak meridional temperature gradient. The deficient simulation of the meridional eddy heat fluxes, which are too strong over large areas of the Southern Ocean, also affects the baroclinic conversion and, consequently, the eddy kinetic energy.

Despite its coarse resolution, LR simulates the more significant patterns of the large-scale circulation reasonably well. In addition, it is able to qualitatively reproduce the interaction between eddies and zonal mean flow. LR tends to overestimate the mean baroclinicity in the region of the main storm track (near 50 °S over the Indian Ocean), but underestimates the baroclinic conversion. Not surprisingly, transient eddies are extremely weak in LR and their contribution to the strengthening of the midlatitude zonal flow is less than in HR. In comparison with HR, the decreased resolution of LR tends to reduce the agreement with the observational-based climatology, but not universally. Between the latitudes of the subtropical jet and the storm track, most of the systematic errors of HR are also present, though the biases tend to be augmented in LR. However,

poleward of the main storm track, LR seems to give better agreement with climatology: the polar jet is less overestimated; the maxima of the eddy kinetic energy and of the EP flux divergence are qualitatively better positioned in LR; and even the equatorward eddy momentum flux and the baroclinic conversion around Antarctica are improved in LR.

Compared with LR, the enhanced resolution experiment improves agreement with climatology, especially in the poleward eddy momentum flux, while the increment in kinetic energy is less pronounced. The discrepancy between the levels of momentum flux and kinetic energy could be related with systematic errors in the baroclinic waves structure (Boyle 1993). This error worsens with increasing resolution as the eddy momentum fluxes increase more rapidly than the kinetic energy (Boville 1991; Carril 1998).

The horizontal resolution is an important factor influencing the model results. Nevertheless, high resolution may not to be sufficient to remedy all problems, because models are very sensitive to many parametrizations and also because many physical schemes could be time step and resolution dependent. Most of the main systematic errors in the models simulations are independent of resolution. In general, increasing resolution tends to increase the model eddy kinetic energy, but results for temperature, moisture and clouds depend on the approach taken to retune the model as resolution is increased (e.g., Stratton 1996). Williamson et al. (1995) studying the dependence on horizontal resolution in the CCM2 GCM found that convergence of statistics which governs the extratropical climate is achieved around T63 (about 1.8°); the remaining changes above this resolution are small in magnitude. Although they concluded that high resolution experiments are needed to capture the nonlinear processes that force the medium scales, other studies (e.g., Tzeng et al. 1993) suggest that even coarse resolution models are suitable tools in particular areas of research (especially in studies of century time scales), when they are able to represent a number of aspects of synoptic systems with useful accuracy. Simmonds and Wu (1993) and Menéndez et al. (1999) suggested that low resolution models are capable of providing guidance as to the way in which the real atmosphere works. We have re-examined and supported this assumption when a model is run with an horizontal mesh stretched over the main baroclinic area of the southern extratropics.

The stretched-grid model presented here has a direct potential for sea surface temperature forced climate change experiments and impact studies focused on the southern extratropics. Progress is expected in the simulation of both synoptic features and the magnitude of eddy statistics with the use of higher resolution. However, the results of this study suggest that at least equally important is the role of the model physics. Physical parametrizations have apparent deficiencies in current GCMs. In this sense, improvements in the physical parametrizations of radiation, convection and vertical diffusion in the free atmosphere can increase the simulated eddy kinetic energy (e.g., Bengtsson 1992). Improving the simulation of eddy properties requires a better understanding and a better handling of complex feedback mechanisms, particularly the processes governing the SH storm tracks. The complex interactions between the various subgrid processes in the southern extratropics need further investigation.

Acknowledgements This paper was partially supported by European Community (CT94-0111) and FONCYT, Argentina (PICT97-583B). Part of the experiments presented here were executed at LMD by Dr. Zhao-Xin Li, who also provide us with the technical support to install the model at CIMA. We especially appreciate his collaboration.

References

Bengtsson LO (1992) Climate system modeling prospects. In: Trenberth KE (ed) Climate system modeling, Cambridge University Press, Cambridge, pp 705–724

Boer GJ, Denis B (1997) Numerical convergence of the dynamics of a GCM. Clim Dyn 13: 359–374

Boer GJ, Arpe K, Blackburn M, Déqué M, Gates WL, Hart TL, Le Treut H, Roeckner E, Sheinin DA, Simmonds I, Smith RNB, Tokioka T, Wetherald RT, Williamson D (1992) Some results from an intercomparison of the climates simulated by 14 atmospheric general circulation models. J Geophys Res 97: 12,771–12,786

Boville BA (1991) Sensitivity of simulated climate to model resolution. J Clim 4: 469–483

Boyle JS (1993) Sensitivity of dynamical quantities to horizontal resolution for a climate simulation using the ECMWF (Cycle 33) model. J Clim 6: 796–813

Carril AF (1998) Estudios de sensibilidad climática en el Hemisferio Sur de acuerdo al modelo de circulación general LMDZ/CIMA. PhD Thesis, University of Buenos Aires, Argentina

Chen B, Bromwich DH (1995) High latitude pressure patterns simulated by global climate models. Proc. First Int AMIP Scientific Conf, WCRP-92, WMO/TD 732

Cotê J, Roch M, Staniforth A, Fillion L (1993) A variable resolution semi-Lagrangian finite-element global model of shallow-water equations. Mon Weather Rev 121: 231–243

Courant R, Friedrichs KO, Lewy H (1928) Uber die partiellen differenzengleichungen der mathematischen physik. Math Annal 100: 67–108

Courtier P, Geleyn J-F (1988) A global numerical weather prediction model with variable resolution: application to the shallow-water equations. Q J R Meteorol Soc 114: 1321–1346

Déqué M, Piedelièvre JP (1995) High resolution simulation over Europe. Clim Dyn 11: 321–339

Fouquart I, Bonnel B (1980) Computations of solar heating of the earth's atmosphere: a new parametrization. Beitr Phys Atmos 53: 35–62

Fox-Rabinovitz MS, Stenchikov GL, Suarez MJ, Takacs LL (1997) A finite-difference GCM dynamical core with a variable resolution stretched grid. Mon Weather Rev 125: 2943–2968

Gates WL, Henderson-Sellers A, Boer GJ, Folland CK, Kitoh A, McAvaney BJ, Semazzi F, Smith N, Weaver AJ, Zeng Q-C (1995) Climate models – evaluation. In: Houghton JT, Meira Filho LG, Callander BA, Harris N, Kattenberg A, Maskell K (eds). Climate change 1995, the science of climate change. Contribution of Working Group I to the Second Assessment Report of the Intergovernmental Panel on Climate Change. WMO/UNEP. Cambridge University Press, Cambridge, UK, pp 228–284

Gates WL (1992) AMIP: the Atmospheric Model Intercomparison Project. Bull Am Meteorol Soc 73: 1962–1970

Held IM, Phillips PJ (1993) Sensitivity of the eddy momentum flux to meridional resolution in atmospheric GCM. J Clim 6: 499–507

Hoskins BJ, Valdés PJ (1990) On the existence of storm-tracks. J Atmos Sci 47: 1854–1864

Hoskins BJ, James IN, White GH (1983) The shape, propagation, and mean flow interaction of large-scale weather systems. J Atmos Sci 40: 977–988

James IN (1994) Introduction to circulating atmospheres. Dessler AJ, Houghton JT, Rycroft MJ (eds). Cambridge Atmospheric and Space Sciences Series

Jones WJ, Hamilton K, Wilson RJ (1997) A very high resolution general circulation model simulation of the global circulation in Austral winter. J Atmos Sci 54: 1107–1116

Katzfey JJ, McInnes KL (1996) GCM simulations of eastern Australian cutoff lows. J Clim 9: 2337–2355

Krinner G, Genthon C, Li Z-X, Le Van P (1997) Studies of the Antarctic climate with a stretched-grid general circulation model. J Geophys Res 102: 13,731–13,745

Kuo H (1965) On formation and intensification of tropical cyclones through latent heat release by cumulus convection. J Atmos Sci 22: 40–63

Kushnir Y, Wallace JM (1989) Interaction of low- and high-frequency transients in a forecast experiment with a general circulation model. J Atmos Sci 46: 1411–1418

Le Treut H, Li ZX (1991) Sensitivity of an atmospheric general circulation model to prescribed SST changes: feedback effects associated with the simulation of cloud optical properties. Clim Dyn 5: 175–187

Manabe S, Smagorinsky J, Stricker RF (1965) Simulated climatology of a general circulation model with hydrologic cycle. Mon Weather Rev 93: 769–798

Manabe S, Smagorinsky J, Holloway JL, Stone HM (1970) Simulated climatology of a general circulation model with a hydrologic cycle. III: effects of increased horizontal computation resolution. Mon Weather Rev 98: 175–212

Meehl GA, Albrecht BA (1988) Tropospheric temperatures and Southern Hemisphere circulation. Mon Weather Rev 116: 953–960

Menéndez CG, Serafini V, Le Treut H (1999) The storm tracks and the energy cycle of the Southern Hemisphere: sensitivity to sea-ice boundary conditions. Ann Geophysicae 17: 1478–1492

Morcrette JJ (1991) Cloud and radiation fields in the ECMWF model: dependence of model horizontal resolution of moist processes. IAMAP Progr Abst, XX General Assembly IUGG, Vienna, Austria

Orlanski I, Sheldon J (1995) Stages in the energetics of baroclinic systems. Tellus 47A: 605–628

Orlanski I, Katzfey JJ, Menéndez CG, Marino M (1991) Simulation of an extratropical cyclone in the Southern Hemisphere: Model sensitivity. J Atmos Sci 48: 2293–2311

Peixoto JP, Oort AH (1992) Physics of climate. American Institute of Physics

Pfeffer RL (1981) Wave-mean flow interactions in the atmosphere. J Atmos Sci 38: 1340–1359

Phillips TJ, Corsetti LC, Grotch SL (1995) The impact of horizontal resolution on moist processes in the ECMWF model. Clim Dyn 11: 85–102

Sadourny R, Laval K (1984) January and July performance of the LMD general circulation model. In: Berger A, Nicolis C (eds) New perspectives in climate modeling. Elsevier, Amsterdam

Senior CA (1995) The dependence of climate sensitivity on the horizontal resolution of a GCM. J Clim 8: 2860–2880

Simmonds I (1990) Improvements in general circulation model performance in simulating Antarctic climate. Antarctic Sci 2: 287–300

Simmonds I, Wu X (1993) Cyclone behavior response to changes in winter southern hemisphere sea-ice concentration. Q J R Meteorol Soc 119: 1121–1148

Sinclair MR (1994) An objective cyclone climatology for the Southern Hemisphere. Mon Weather Rev 121: 941–960

Staniforth A, Mitchell H (1978) A variable resolution finite element technique for regional forecasting with primitive equations. Mon Weather Rev 106: 439–447

Staniforth A, Cotê J, Fillion L, Roch M (1991) A variable resolution finite element semi-Lagrangian global model of the shallow water equations. Preprints Ninth Conf Numerical Weather Prediction, Denver, CO, AMS, 621–622

Stendel M, Roeckner E (1998) Impacts of horizontal resolution on simulated climate statistics in ECHAM 4, Max-Plank-Institut fur Meteorologie, Report 253, Hamburg

Stephenson DB, Held IM (1993) GCM response of northern winter stationary waves and storm tracks to increasing amounts of carbon dioxide. J Clim 6: 1859–1870

Stratton RA (1996) A high resolution AMIP run using the Hadley Centre model HadAM2b. CRTN 77, Hadley Centre, UK

Trenberth KE (1980) Planetary waves at 500 mb in the Southern Hemisphere. Mon Weather Rev 108: 1378–1389

Trenberth KE (1981) Observed Southern Hemisphere eddy statistics at 500 mb: Frequency and Spatial Dependence. J Atmos Sci 38: 2585–2603

Trenberth KE (1986) An assessment of the impact of transient eddies on the zonal flow during a blocking episode using localized Eliassen-Palm flux diagnostics. J Atmos Sci 43: 2070–2087

Trenberth KE (1991) Storm tracks in the Southern Hemisphere. J Atmos Sci 48: 2159–2178

Tzeng R, Bromwich DH, Parish TR (1993) Present-day Antarctic climatology of the NCAR Community Climate Model Version 1. J Clim 6: 205–226

van Loon H (1979) The association between latitudinal temperature gradient and eddy transport. Part I: transport of sensible heat in winter. Mon Weather Rev 107: 525–534

van Loon H, Jenne RL (1972) The zonal harmonic standing waves in the Southern Hemisphere. J Geophys Res 77: 992–1003

Wellck RE, Kasahara A, Washington WM, Santo GD (1971) Effect of horizontal resolution in finite-difference model of the general circulation. Mon Weather Rev 99: 673–683

Whetton PH, Pittock AB, Labraga JC, Mullan AB, Joubert A (1996) Southern Hemisphere Climate: Comparing models with reality. In: Gianbelluca T, Henderson-Sellers A (eds), Climate change, people and policy: developing Southern Hemisphere Perspectives. John Wiley and Sons, Chichester pp 89–130

Williamson DL, Kiehl JT, Hack JJ (1995) Climate sensitivity of the NCAR Community Climate Model (CCM2) to horizontal resolution. Clim Dyn 11: 377–397

Xu J-S, von Storch H, van Loon H (1990) The performance of four spectral GCMs in the Southern Hemisphere: the January and July climatology and the semi-annual wave. J Clim 3: 53–70

Yessad K, Benard P (1996) Introduction of local mapping factor in the spectral part of the Meteo-France global variable mesh numerical forecast model. Q J R Meteorol Soc 122: 1701–1719